Mutations in the *Saccharomyces cerevisiae* Type 2A Protein Phosphatase Catalytic Subunit Reveal Roles in Cell Wall Integrity, Actin Cytoskeleton Organization and Mitosis

David R. H. Evans and Michael J. R. Stark

Department of Biochemistry, University of Dundee, Dundee, United Kingdom

Manuscript received June 24, 1996
Accepted for publication November 1, 1996

ABSTRACT

Temperature-sensitive mutations were generated in the *Saccharomyces cerevisiae PPH22* gene that, together with its homologue *PPH21*, encode the catalytic subunit of type 2A protein phosphatase (PP2A). At the restrictive temperature (37°), cells dependent solely on *pph22*^{ts} alleles for PP2A function displayed a rapid arrest of proliferation. Ts$^-$ *pph22* mutant cells underwent lysis at 37°, showing an accompanying viability loss that was suppressed by inclusion of 1 M sorbitol in the growth medium. Ts$^-$ *pph22* mutant cells also displayed defects in bud morphogenesis and polarization of the cortical actin cytoskeleton at 37°. PP2A is therefore required for maintenance of cell integrity and polarized growth. On transfer from 24° to 37°, Ts$^-$ *pph22* mutant cells accumulated a 2N DNA content indicating a cell cycle block before completion of mitosis. However, during prolonged incubation at 37°, many Ts$^-$ *pph22* mutant cells progressed through an aberrant nuclear division and accumulated multiple nuclei. Ts$^-$ *pph22* mutant cells also accumulated aberrant microtubule structures at 37°, while under semi-permissive conditions they were sensitive to the microtubule-destabilizing agent benomyl, suggesting that PP2A is required for normal microtubule function. Remarkably, the multiple defects of Ts$^-$ *pph22* mutant cells were suppressed by a *viable* allele (*SSD1-v1*) of the polymorphic *SSD1* gene.

PROTEIN phosphatase type 2A (PP2A) is one of three major protein serine/threonine phosphatases that are phylogenetically conserved in eukaryotic cells (COHEN 1989; COHEN *et al.* 1989). The core of PP2A consists of a 36-kDa catalytic (C) subunit bound to a 65-kDa regulatory A subunit. This core associates in turn with regulatory B subunits of various sizes, forming a trimeric complex (COHEN 1989). The yeast *Saccharomyces cerevisiae* contains two redundant genes, *PPH21* and *PPH22*, encoding proteins displaying ~80% amino acid sequence identity to the C subunit of mammalian PP2A (SNEDDON *et al.* 1990; RONNE *et al.* 1991). Deletion of both *PPH21* and *PPH22* causes a severe growth defect but in most strain backgrounds is not lethal (RONNE *et al.* 1991). However, deletion of both genes *is* lethal in combination with loss of *PPH3*, a gene that encodes a further protein phosphatase catalytic subunit (RONNE *et al.* 1991). This suggests that the Pph3 phosphatase provides some function overlapping with that of PP2A, despite being only moderately related to the *PPH21* and *PPH22* gene products both in amino acid sequence (RONNE *et al.* 1991) and enzymatic properties (HOFFMANN *et al.* 1994). Deletion of *PPH3* alone causes no apparent effect on cell growth and division (RONNE *et al.* 1991) and thus both the physiological role of Pph3p and its relationship to PP2A are unclear.

Corresponding author: Michael J. R. Stark, Department of Biochemistry, The University, Dundee, DD1 4HN, United Kingdom.
E-mail: m.j.r.stark@dundee.ac.uk

Morphogenesis in *S. cerevisiae* involves a highly polarized mode of vegetative cell growth via budding, during which newly synthesized materials are delivered to a preselected site on the cell surface (CHANT 1994). Directed cell growth is accompanied by polarization of actin (ADAMS and PRINGLE 1984; KILMARTIN and ADAMS 1984; LEW and REED 1993), suggesting that microfilaments organize the vectorial transport of materials to sites of new cell growth. PP2A has been implicated in yeast morphogenesis because overexpression or depletion of Pph22p affects bud morphology (RONNE *et al.* 1991) and *pph21* mutations disrupt both bud morphogenesis and the polarized distribution of the actin cytoskeleton (LIN and ARNDT 1995). Similarly, mutants defective for the Cdc55p (HEALY *et al.* 1991) or Tpd3p (VAN ZYL *et al.* 1992) regulatory subunits of PP2A display an elongated bud morphology and are defective for septation and/or cell separation, generating multiply budded cells under nonpermissive conditions. Consistently, mutations in the genes for the A and B regulatory subunits of fission yeast PP2A cause defects in cell wall synthesis, cytokinesis or cell separation and the actin cytoskeleton (KINOSHITA *et al.* 1996). Thus the role of PP2A in cellular morphogenesis is conserved between distantly related organisms.

Several studies have suggested a role for PP2A in the regulation of mitosis. In *S. cerevisiae*, mutation of *PPH21* inhibits entry into mitosis (LIN and ARNDT 1995), suggesting that PP2A plays a positive role. In contrast, stud-

ies performed in other systems have revealed a negative role for PP2A in mitotic regulation. Thus PP2A C subunit mutations in *Schizosaccharomyces pombe* caused premature mitosis (KINOSHITA *et al.* 1990, 1993) and a form of PP2A (termed INH) purified from immature Xenopus oocytes inhibits activation of cdc2 kinase, preventing exit from G2 (LEE *et al.* 1991, 1994). In addition, a mutation in the 55-kDa B subunit (PR55) of Drosophila PP2A inhibits progression through anaphase (MAYER-JAEKEL *et al.* 1993). Thus, either there may be more than one role of PP2A in mitosis or the precise role may vary between different organisms.

The *S. cerevisiae SSD1* gene is polymorphic (SUTTON *et al.* 1991) and encodes a polypeptide with similarity to the *S. pombe* mitotic regulatory protein dis3 (KINOSHITA *et al.* 1991). *SSD1* was identified as a suppressor of mutations in *SIT4*, which encodes a protein phosphatase displaying 55% amino-acid sequence identity to the mammalian PP2A C subunit (SUTTON *et al.* 1991). Sit4p function is required for expression of G1 cyclins that promote the execution of Start and for bud formation (FERNANDEZ-SARABIA *et al.* 1992). Deletion of *SIT4* is lethal in an *ssd1-d*, but not an *SSD1-v*, background. Furthermore, *SSD1* influences the phenotype of several mutants defective for cell growth and morphogenesis. For example, *SSD1-v* alleles suppress mutations in the protein kinase C signaling pathway (see DOSEFF and ARNDT 1995), which is involved in polarized growth and cell wall synthesis (ERREDE and LEVIN 1993). However, the role of *SSD1* in cell growth and morphogenesis is poorly understood.

In this study we have investigated the effects of PP2A rapid loss-of-function by examining the phenotype of temperature-sensitive strains of *S. cerevisiae* mutated for the *PPH22* gene. The phenotype of Ts$^-$ *pph22* mutant cells is consistent with a role for PP2A in both polarized cell growth and nuclear division. In addition, we have explored the influence of the *PPH3* and *SSD1-v1* genes on PP2A function and find that both genes partially suppress the effects of *pph22*^{ts} mutations.

MATERIALS AND METHODS

Strains, plasmids, media and genetic techniques: Strains and plasmids are listed in Table 1 and Table 2, respectively. The pRS (SIKORSKI and HIETER 1989), YCplac (GIETZ and SUGINO 1988), YDp (BERBEN *et al.* 1991) and pBSII KS+ (Stratagene) vectors have been described. Yeast cells were grown in rich (YEPD), synthetic minimal (SD), or 5-fluoroorotic acid (5-FOA) medium, and *lys2* mutants were selected on medium containing α-aminoadipate (KAISER *et al.* 1994). Standard procedures were employed for DNA manipulations (SAMBROOK *et al.* 1989) and genetic methods (KAISER *et al.* 1994). Yeast transformations followed the method of SCHIESTL and GIETZ (1989). All marker integrations were verified by appropriate Southern blot analysis.

Microscopy, flow cytometry and measurement of cellular parameters: Cellular components were examined by fluorescence and indirect immunofluorescence microscopy as described by KAISER *et al.* (1994). Actin was visualized using rhodamine-phalloidin (Molecular Probes). Tubulin was visualized using the primary antibody YOL1/34 (Sera Lab) at a dilution of 1:50 and a secondary, fluorescein isothiocyanate-conjugated goat anti-rat antibody (Sigma) at a dilution of 1:20. Flow cytometry was performed as described previously (BUTLER *et al.* 1991) using a Becton Dickinson FACScan and data was analyzed using the Lysis II software. Yeast cell number was determined using a hemacytometer. To determine cell viability, cells were sonicated and diluted in phosphate-buffered saline (PBS; SAMBROOK *et al.* 1989), and 100-μl samples were spread onto YEPD medium and incubated for 3 days at 24°. When cells were grown in osmotically stabilized medium, they were diluted in 1 M sorbitol for viability measurements.

Gene deletion constructs: The *pph21::LEU2* (SNEDDON *et al.* 1990) and *pph22Δ1::HIS3* (SUTTON *et al.* 1991) alleles have been described. The *pph21Δ1::HIS3* allele (pDE211) was constructed by replacing the 1012-bp *PPH21 Eco*RI/*Nsi*I fragment [encoding 90% of the *PPH21* open reading frame (ORF)] with the ~1000 bp *HIS3 Eco*RI/*Nsi*I fragment from plasmid YDp-H. To construct the *pph22Δ1::URA3* allele (plasmid pDE10), the 1.4-kb *PPH22 Bst*BI fragment (encompassing the entire *PPH22* ORF) was removed from pDE22 and the plasmid was recircularized by blunt-end ligation (generating an *Nru*I site) after treatment with Klenow fragment. A 1.1-kb *Sma*I fragment containing *URA3* from pDE8 was then inserted at the unique *Nru*I site. A *pph3Δ1::LYS2* allele was constructed by replacing the 4.8-kb *Bsa*AI fragment (encompassing the *PPH3* ORF) with the 5-kb *LYS2 Sal*I/*Hin*dIII fragment from YDp-K, generating plasmid pph3ΔLYS2.

Construction of a *pph21Δ1::HIS3 pph22Δ1::URA3* double mutant: pDE10 (*pph22Δ1::URA3*) was cleaved with *Xba*I/*Eco*RI and used to transform strain ASY927 to Ura$^+$. Tetrad analysis of one transformant (DEY10) confirmed 2:2 segregation of the deletion, and one *pph22Δ1::URA3* segregant (DEY10-2B) was crossed with the *pph21Δ1::HIS3* deletion strain DEY132-1C. Sporulation and tetrad analysis of the resultant diploid (DEY1032) confirmed the expected linkage between *pph21Δ1::HIS3* and *pph22Δ1::URA3* alleles (29 cM, n = 60 asci) and generated the double mutant DEY1032-2C.

Mutagenesis of the *PPH22* gene: *PPH22* was amplified under mutagenic conditions (LEUNG *et al.* 1989) for PCR. PCR reactions contained 20 ng of plasmid YCpDE8 template, 1× reaction buffer without $MgCl_2$ (Promega), 200 ng forward primer (5′-CCAGATCTGTGGAAAAGAGTCGTGG), 200 ng reverse primer (5′-CCAGATCTGGAGTGAACTATACATAGCG), 0.1 mM each dATP and dGTP, 0.5 mM each dTTP and dCTP, 2.0–3.0 mM $MgCl_2$, 0.1–0.3 mM $MnCl_2$ and 5 U *Taq* DNA polymerase (Promega). Reactions were subjected to 33 cycles of 94° for 1 min, 52° for 2.5 min and 72° for 5 min. Mutant alleles were recovered according to MUHLRAD *et al.* (1992), cotransforming competent cells of strain DEY1 with mutagenic PCR product (100–250 ng) and *Bst*BI-cleaved YCpDE2 plasmid DNA (100 ng). Trp$^+$ transformants (3000) were selected on medium lacking tryptophan and uracil, then transferred to medium containing uracil to promote loss of YCpDE8. Ura$^-$ segregants (600) were selected on 5-FOA medium, transferred to YEPD medium and incubated at 22° or 37° to screen for temperature sensitivity. Nine plasmids supporting temperature-sensitive cell growth were recovered into *Escherichia coli*, and the Ts$^-$ phenotype they conferred was verified by plasmid shuffling using strain DEY1.

Construction of *pph22*^{ts} alleles containing single missense mutations: The multiple missense mutations encoded by the *pph22-1*, *pph22-17* and *pph22-19* alleles (Table 3) were separated by subcloning. The 737-bp *Kpn*I/*Bst*XI and 914-bp *Bst*XI/*Eco*RI fragments from the *pph22-1* allele were used to replace separately the homologous fragments of wild-type *PPH22*, generating the novel alleles *pph22-11* and *pph22-12*, respectively. Similarly, the 344-bp *Bst*XI/*Sac*I and 478-bp *Bst*EII/*Eco*RI fragments from *pph22-19* were used to replace

TABLE 1

Yeast strains

Strain	Genotype	Source
AY925	*MAT***a** W303[a]	K. ARNDT
AYS927	*MAT***a**/*MATα* W303	BLACK *et al.* (1995)
DEY1	*MAT***a** *pph22Δ1::HIS3 pph21::LEU2 pph3Δ1::LYS2 lys2-951* [YCpAS6 *PPH22*] W303	This study
DEY3	*MAT***a** *pph22Δ1::HIS3 pph21::LEU2 pph3Δ1::LYS2 lys2-951* [YCpDE8 *PPH22*] W303	This study
DEY10	*MAT***a**/*MATα* *pph22Δ1::URA3*/+ W303	This study
DEY10-2B	*MATα* *pph22Δ1::URA3* W303	From DEY10
DEY100	*MAT***a** *pph22-12 pph21Δ1::HIS3 pph3Δ1::LYS2 lys2-952* W303	This study
DEY102D	*MAT***a**/*MATα* *pph22-12/pph22-12 pph21Δ1::HIS3/pph21Δ1::HIS3 pph3Δ1::LYS2/pph3Δ1::LYS2 lys2-952/lys2-952* W303	This study
DEY103D	*MAT***a**/*MATα* *pph21Δ1::HIS3/pph21Δ1::HIS3 pph3Δ1::LYS2/pph3Δ1::LYS2 lys2-952/lys2-952* W303	This study
DEY132	*MAT***a**/*MATα* *PPH22::URA3*/+ *pph21Δ1::HIS3*/+ W303	This study
DEY132-1C	*MAT***a** *pph21Δ1::HIS3* W303	From DEY132
DEY132-2B	*MAT***a** *PPH22::URA3 pph21Δ1::HIS3* W303	From DEY132
DEY142	*MAT***a**/*MATα* *pph22-12::URA3*/+ *pph21Δ1::HIS3*/+ W303	This study
DEY142-1C	*MAT***a** *pph22-12::URA3 pph21Δ1::HIS3* W303	From DEY142
DEY172	*MAT***a**/*MATα* *pph22-172::URA3*/+ *pph21Δ1::HIS3*/+ *lys2-952*/+ W303	This study
DEY172-2B	*MAT***a** *pph22-172::URA3 pph21Δ1::HIS3 lys2-952* W303	From DEY172
DEY213	*MAT***a** *PPH22::URA3 pph21Δ1::HIS3 pph3Δ1::LYS2 lys2-953* W303	From DEY132-2B
DEY214	*MAT***a** *pph22-12::URA3 pph21Δ1::HIS3 pph3Δ1::LYS2 lys2-952* W303	From DEY142-1C
DEY217	*MAT***a** *pph22-172::URA3 pph21Δ1::HIS3 pph3Δ1::LYS2 lys2-952* W303	From DEY172-2B
DEY292	*MAT***a**/*MATα* *pph22-12::URA3*/+ *pph21Δ1::HIS3*/+ *pph3Δ1:LYS2*/+ *lys2-952*/*lys2-952* W303	This study
DEY293-42C	*MAT***a** *mpk1Δ1::TRP1* W303	This study
DEY926	*MATα* *lys2-954* W303	This study
DEY1032-2C	*MAT*? *pph22Δ1::URA3 pph21Δ1::HIS3* W303	This study
DEY9142	*MAT***a**/*MATα* *pph21Δ1::HIS3*/+ *lys2-954*/+ W303	From DEY926 × DEY132-1C

[a] Isogenic with strain W303 (*ade2-1 ura3-1 his3-11 trp1-1 leu2-3,112 can1-100 ssd1-d2*).

TABLE 2

Plasmids

Plasmid	Description	Source
YCpDE8	*PPH22* 1.8-kb *Xba*I/*Eco*RI fragment in pRS316	This study
YCpDE1	*PPH22* 1.8-kb *Xba*I/*Eco*RI fragment in YCplac22	This study
YCpDE2[a]	*pph22Δ* 0.4-kb *Xba*I/*Eco*RI fragment in YCplac22	This study
pDE211	*pph21Δ1::HIS3* 2.3-kb *Xho*I/*Xba*I fragment in pBSII KS+	This study
pDE10	*pph22Δ1::URA3* 1.5-kb *Xba*I/*Eco*RI fragment in pBSII KS+	This study
pDE22	*PPH22* 1.8-kb *Sal*I/*Eco*RI fragment in pBSII KS+	This study
pph3ΔLYS2	*pph3Δ1::LYS2* 5.5-kb *Hin*dIII fragment in pBS KS−	A. SNEDDON
pDE14	*pph22-12::URA3* 2.9-kb *Xba*I/*Eco*RI fragment in pBSII KS+	This study
pDE13	*PPH22::URA3* 2.9-kb *Xba*I/*Eco*RI fragment in pBSII KS+	This study
pDE17	*pph22-172::URA3* 2.9-kb *Xba*I/*Eco*RI fragment in pBSII KS+	This study
pDE8[b]	*URA3* 1.6-kb *Ssp*I/*Nhe*I fragment from YDp-U in pBSII KS+ (*Ssp*I/*Spe*I)	This study
YIpDE22-12	*pph22-12* 1.8-kb *Xba*I/*Eco*RI fragment in YIplac128	This study
pDE22-12	*pph22-12* 1.8-kb *Xba*I/*Eco*RI fragment in pBSII KS+	This study
pBR322-(*mpk1::TRP1*)	*mpk1::TRP1* 2.9-kb *Sal*I/*Eco*RI fragment in pBR322	D. LEVIN
pTS64	*SSD1-v1* 6.0-kb *Sph*I fragment in pRS315	W. HILT
YCpDE24	*SSD1-v1* 4.3-kb *Sac*I/*Sal*I fragment in pRS314	This study
YCpDE22	*PPH22* 1.8-kb *Sal*I/*Eco*RI fragment in pRS315	This study

[a] YCpDE2 was generated by removing the 1.4-kb *Bst*BI fragment (containing the complete *PPH22* ORF) from YCpDE1. Digestion of YCpDE2 with *Bst*BI generates a linear *pph22* gapped plasmid.

[b] *URA3* 1.6-kb cassette excised by *Sma*I digestion.

TABLE 3

Mutational changes in *pph22*^{ts} alleles

Allele[a]	Parental allele	Mg^{2+}/Mn^{2+} in PCR (mM)[b]	Base change	Amino acid change	Ts^- phenotype[c]
pph22-11	*pph22-1*	3.0/0.1	A281 → T	D94V	No
pph22-12	*pph22-1*	3.0/0.1	T695 → C	F232S	Yes
pph22-171	*pph22-17*	3.0/0.2	A79 → G; C192 → A	S27G; silent	No
pph22-172	*pph22-17*	3.0/0.2	C719 → A	P240H	Yes
pph22-173	*pph22-17*	3.0/0.2	T1129 → A	L377I	No
pph22-191	*pph22-19*	3.0/0.2	T603 → C; A889 → T	Silent; N297Y	No[d]
pph22-192	*pph22-19*	3.0/0.2	T1041 → G	D347E	No[d]
—	*pph22-19*	3.0/0.2	T15 → A; C192 → A; A942 → G	All silent	—

[a] See MATERIALS AND METHODS for details of subcloning.
[b] $MgCl_2$ (Mg^{2+}) and $MnCl_2$ (Mn^{2+}) concentrations used for the mutagenic PCR.
[c] Plasmid-borne *pph22* alleles were shuffled into strain DEY1 and tested for growth on rich medium at 37°.
[d] Both amino acid substitutions encoded by *pph22-19* were needed for temperature sensitivity.

the equivalent *PPH22* fragments, generating the *pph22-191* and *pph22-192* alleles, respectively. The 859-bp *Xba*I/*Bst*XI, 436-bp *Bst*XI/*Bst*EII and 570-bp *Sac*I/*Eco*RI fragments from *pph22-17* were used similarly to generate the *pph22-171, pph22-172* and *pph22-173* alleles, respectively. Each novel *pph22* allele was inserted into a *CEN* vector as a 1.8-kb *Xba*I/*Eco*RI fragment and verified by nucleotide sequence analysis.

Marking of the *pph22-12, pph22-172* and *PPH22* alleles: The 1.1-kb *Sma*I *URA3* fragment from pDE8 was inserted at the unique *Sna*BI site downstream of each of the *pph22-12, pph22-172* and *PPH22* coding regions in DNA containing no apparent ORFs, generating pDE14, pDE17 and pDE13, respectively. These marked alleles were then integrated at the homologous genomic locus. For *pph22-12::URA3,* strain AYS927 was transformed to Ura^+ using the 2.9-kb *Xba*I/*Eco*RI fragment of pDE14. A *pph22-12::URA3*/+ transformant was next deleted for one copy of *PPH21* by transformation to His^+ using the 2.7-kb *Xba*I/*Xho*I fragment of pDE211 (*pph21Δ1::HIS3*). One transformant (DEY142) showed 2:2 segregation of both markers and linkage (24 cM, $n = 28$ asci) as expected (SNEDDON *et al.* 1990), consistent with heterozygosity for both *pph22-12::URA3* and *pph21Δ::HIS3*. To generate a *pph22-12::URA3 pph21Δ pph3Δ* triple mutant, a *lys2* derivative of a haploid DEY142 segregant (DEY142-1C) was transformed to Lys^+ using the 5.5-kb *Hin*dIII fragment from plasmid pph3ΔLYS2. An appropriate transformant (DEY214) was identified that showed 2:2 segregation of *pph3Δ1::LYS2*. Isogenic strains (DEY132-2B, DEY213) in which the wild-type *PPH22* allele was marked with *URA3* were obtained and verified as above but using the 2.9-kb *Xba*I/*Eco*RI fragment from pDE13. A strain containing an unmarked *pph22-12* allele was made by removing the *URA3* gene flanking *pph22-12* in strain DEY214. Accordingly, YIpDE22-12 (*LEU2 pph22-12*) was linearized at the unique *Sac*I site in the *pph22-12* ORF and integrated into strain DEY214. A Leu^+ transformant was identified that generated Leu^-, Ura^- recombinants when plated on 5-FOA medium due to recombination between the duplicated 3′ regions of *pph22-12*. Southern blot and PCR analysis verified that one such recombinant (DEY100) contained an unmarked *pph22-12* allele.

To integrate a *pph22-172::URA3* allele, the 2.9-kb *Xba*I/*Eco*RI fragment from pDE17 was introduced into strain DEY9142, and Ura^+ transformants were selected. A transformant (DEY172) in which a chromosomal *PPH22* gene was replaced by *pph22-172::URA3* was identified and a *pph22-172::URA3 pph21Δ* segregant obtained (DEY172-2B). A *pph22-172::URA3 pph21Δ pph3Δ* derivative (DEY217) was generated using the 5.5-kb *Hin*dIII fragment from plasmid pph3ΔLYS2 as described above. For both the *pph22-12::URA3* and *pph22-172::URA3* alleles, the Ura^+ and Ts^- phenotypes were shown to cosegregate.

Construction of an *mpk1* deletion strain: The 2.1-kb *Sal*I/*Eco*RI fragment from plasmid pBR322-(*mpk1::TRP1*) carrying *mpk1::TRP1* (LEE *et al.* 1993) was introduced into strain DEY292, selecting for Trp^+ transformants. An *mpk1Δ1::TRP1* segregant (DEY293-42C) was identified following tetrad analysis (2:2 segregation of Trp^+ in 41 tetrads).

Trypan blue exclusion assay of cell wall permeability: Cells were grown to a density of $5–7 \times 10^6$/ml in YEPD medium containing 1 M sorbitol at 24° and shifted to 37° for 2 hr. Culture samples (0.5 ml) were then transferred to YEPD medium with or without 1 M sorbitol (4.5 ml, prewarmed to 37°) and incubated for a further 2 hr at 37°. Cells (0.5 ml) were stained with trypan blue (final concentration 0.01%), fixed with formaldehyde (final concentration 3.7%), sonicated lightly and examined by phase contrast microscopy.

***SSD1-v1* plasmid-shuffling in strain DEY3:** Plasmids YCpDE24, YCpDE1 and pRS314 were introduced separately into strain DEY3 and Trp^+ transformants selected. Independent transformants (two for each plasmid) were inoculated into 30 ml minimal medium containing uracil but lacking tryptophan and grown to saturation at 24°. Cells ($\sim 5 \times 10^6$) were spread onto 5-FOA medium and incubated for 1 week at 24°.

RESULTS

Generation and nucleotide sequence analysis of *pph22* temperature-sensitive alleles: To study PP2A rapid loss of function in *S. cerevisiae,* we have generated novel, temperature-sensitive alleles of *PPH22,* one of two redundant genes encoding the PP2A C subunit. These mutant alleles were generated by PCR and identified using a plasmid shuffle method. The temperature-sensitive (Ts^-) phenotype conferred by each *pph22* allele was recessive since it was rescued by low copy *PPH22* (not shown).

We determined the complete nucleotide sequence of three mutant *pph22* alleles (*pph22-1, pph22-17* and *pph22-19*), finding multiple missense mutations in each and additional silent mutations in two of them (Table 3). To determine which of the missense mutations caused Ts^- growth, we replaced fragments of the wild-type *PPH22* gene with homologous fragments derived from the appropriate mutant alleles. These novel, plas-

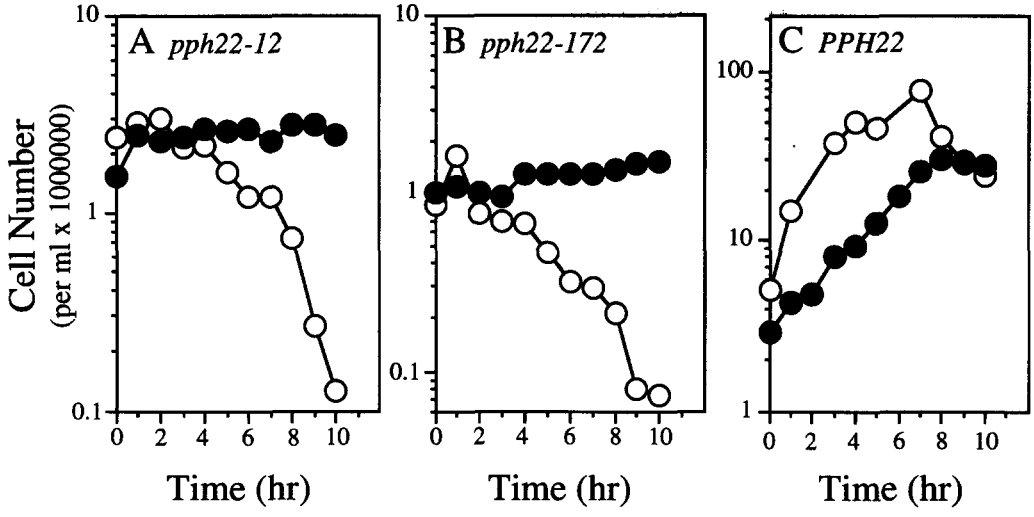

FIGURE 1.—Proliferation and viability of Ts⁻ *pph22* mutants under restrictive conditions. Cultures growing actively in liquid YEPD medium at 24° were transferred to 37° and monitored at hourly intervals for cell number and viability. (A) DEY214; (B) DEY217; (C) DEY213. ●, cell number; ○, viable cells.

mid-borne *pph22* alleles contained individual missense mutations and were introduced separately into strain DEY1 (*pph21*Δ *pph22*Δ *pph3*Δ) by plasmid-shuffling, testing for their ability to confer Ts⁻ growth at 37° (Table 3). Surprisingly, both amino acid substitutions encoded by *pph22-19* were necessary to confer the Ts⁻ phenotype. However, the F232S mutation of *pph22-1* was solely responsible for temperature sensitivity, as was the P240H substitution in *pph22-17*. Mutant alleles encoding only these latter substitutions were named *pph22-12* and *pph22-172*, respectively, and used in all further studies, following integration into the genome at the homologous locus in strains deleted for the redundant gene *PPH21*. We will refer to strains deleted for *PPH21* and containing a mutant *pph22*^{ts} allele as Ts⁻ *pph22* strains. Unless stated otherwise, our Ts⁻ *pph22* strains also lack *PPH3* (see Introduction) and so the mutant *pph22* gene is the only source of PP2A-complementing activity in these cells.

Proliferation and viability of Ts⁻ *pph22* strains: The Ts⁻ *pph22-12* and *pph22-172* strains were subjected to temperature-shift analysis in liquid medium to assess proliferation and viability at 37°. Unlike wild-type cells (Figure 1C), *pph22-12* mutant cells ceased proliferation within one generation following transfer from 24° to 37° (Figure 1A). The level of mutant cell viability remained high at 37° for 2–3 hr, but afterward declined rapidly (Figure 1A). In contrast, wild-type cells retained viability for at least 10 hr at 37° (Figure 1C). Cells containing *pph22-172* also displayed an arrest of proliferation and viability loss at 37° (Figure 1B). On solid YEPD medium, the minimum restrictive temperatures for growth of *pph22-12* and *pph22-172* mutant cells were 37° and 35°, respectively (see Figure 2A), implying that the Pph22 polypeptide is affected more severely by the *pph22-172* mutation. Consistently, *pph22-172* cells arrested proliferation more quickly at 37° and the loss of viability was initially more rapid than in *pph22-12* cells.

Microscopic examination of Ts⁻ *pph22* cultures revealed an accumulation of cell debris at 37° (not shown), suggesting that cell lysis was occurring. We therefore tested the ability of *pph22-12* mutant cells to grow at 37° on medium containing 1 M sorbitol, which serves as an osmotic stabilizing agent capable of rescuing a variety of yeast mutants that undergo temperature-dependent cell lysis (CID *et al.* 1995). In contrast to their lack of growth on YEPD medium at 37°, *pph22-12* mutant cells displayed apparently wild-type growth on sorbitol-containing medium at 37° (Figure 2A, top). Furthermore, analysis performed in liquid medium revealed that the growth rate of *pph22-12* mutant cells at 37° in the presence of 1 M sorbitol was similar to that of wild-type cells (Figure 2B). While sorbitol could not rescue the growth of *pph22-172* cells at 37°, these cells grew well on sorbitol-containing medium at the restrictive temperature of 35°, supporting the idea that the effects of the *pph22-172* allele are more severe. The Ts⁻ phenotype of *pph22* cells was similarly suppressed by 0.5 M KCl as an alternative osmotic stabilizing agent (not shown). These observations are consistent with the notion that Ts⁻ *pph22* cells undergo temperature-dependent cell lysis.

To demonstrate a cell wall integrity defect in the Ts⁻ *pph22* cells at 37° more directly, we made use of a trypan blue exclusion assay. This is based on the ability of wild-type cells to exclude trypan blue dye efficiently upon transfer from hypertonic to hypotonic conditions, whereas under the same conditions cells with a weakened cell wall become dye-permeable (KARPOVA *et al.* 1993). As a control for this experiment, we included a mutant strain deleted for *MPK1*, a gene that encodes a mitogen-activated protein (MAP) kinase homologue involved in the maintenance of yeast cell wall integrity (LEE *et al.* 1993); *mpk1*Δ mutant cells undergo cell lysis at 37°. Table 4 shows that when transferred to osmotically stabilized liquid medium, none of the strains tested showed an appreciable fraction of cells that stained with trypan blue. However, when transferred from YEPD medium containing 1 M sorbitol to YEPD medium alone, ~20% of cells in a *pph22-172* culture were permeable to trypan

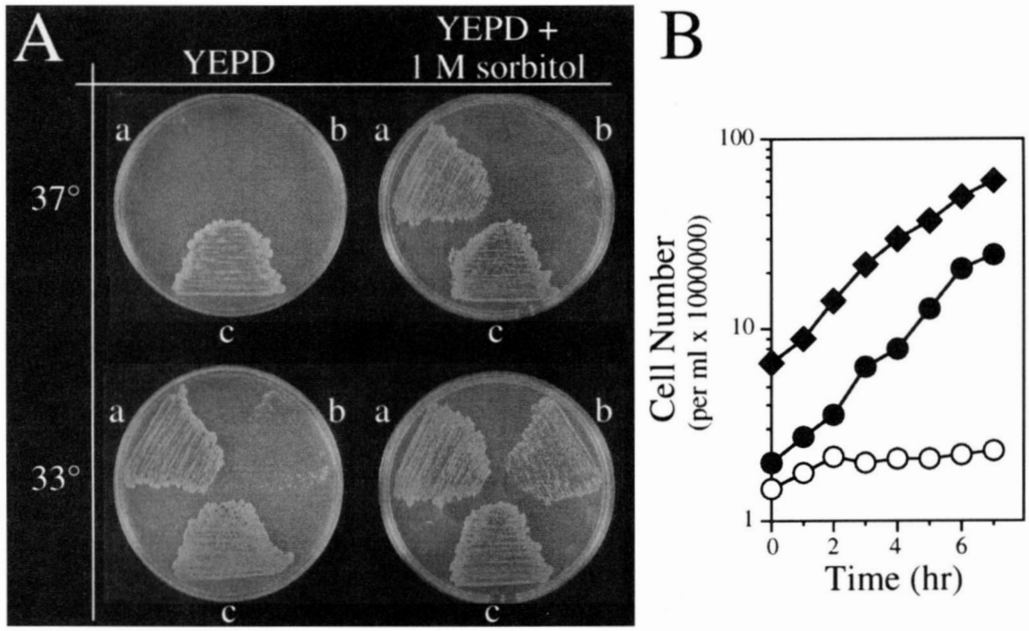

FIGURE 2.—Effect of 1 M sorbitol on the Ts⁻ *pph22* mutant phenotype. (A) Suppression of the *pph22-12* and *pph22-172* Ts⁻ growth defect by 1 M sorbitol. Cells were streaked on either YEPD medium (left) or YEPD medium containing 1 M sorbitol (right) and incubated for 2 days at either 37° (top) or 33° (bottom). (a) *pph22-12* (DEY214); (b) *pph22-172* (DEY217); (c) *PPH22* (DEY213). (B) Growth rate of *pph22-12* mutant cells in medium containing 1 M sorbitol. Cells growing actively at 24° in liquid YEPD medium with or without 1 M sorbitol as indicated were transferred to 37° and monitored hourly for cell density. ◆, *PPH22* (AYS927) in YEPD/1 M sorbitol; ●, *pph22-12* (DEY102D) in YEPD/1 M sorbitol; ○, *pph22-12* in YEPD.

blue at 37°, a sixfold higher fraction than in a wild-type culture and comparable to that of the *mpk1*Δ control strain (Table 4). Thus Ts⁻ *pph22* cells possess a weakened cell wall at 37°, which increases their permeability to dye on hypo-osmotic shock. Taken together, the trypan blue permeability of *pph22* cells and suppression of *pph22* mutant phenotypes by osmotic stabilizing agents indicate that *pph22* mutant cells undergo a temperature-dependent perturbation of cell wall integrity, supporting the notion that cell lysis contributes to the loss of viability displayed by Ts⁻ *pph22* mutant cells at 37°.

Bud morphogenesis and actin deposition in Ts⁻ *pph22* cells: At 24°, <1% of the cells in a *pph22-12* mutant culture displayed aberrant morphologies. In contrast, after 4 hr of incubation at 37°, ~38% of *pph22-12* mutant cells displayed an aberrant bud morphology, with some buds appearing angular, elongated, hook-like or lumpy in shape (Figure 3 and data not shown). In addition, some *pph22-12* mutant cells displayed a thickened neck between the mother cell and bud, while others displayed a wild-type morphology. Many of the abnormal bud morphologies were therefore quite distinct from the pear-shaped buds noted on depletion of PP2A by repression of a *GAL1-PPH22*-dependent strain (RONNE *et al.* 1991) but were essentially identical to the aberrant morphologies described by LIN and ARNDT (1995) for Ts⁻ *pph21-102* mutant cells at the restrictive temperature. Also similar to *pph21-102* cells, *pph22-12* cells displayed a defect in the polarization of cortical actin deposition at 37°. In wild-type cells, cortical actin is associated with regions of active growth and therefore, in small-budded cells, it is localized exclusively to the growing bud (Figure 3A, a–d). At 24°, *pph22-12* mutant cells displayed a wild-type pattern of cortical actin distribution (Figure 3A, e–h). However, at 37°, the cortical actin present in many of the budded *pph22-*

TABLE 4

Cell wall integrity of Ts⁻ *pph22* strains monitored by trypan blue staining

	Percentage of cells staining with trypan blue in different strains[a]			
Treatment[b]	Wild type	*pph22-172*	*pph21*Δ *pph22*Δ	*mpk1*Δ
YEPD/1 M sorbitol → YEPD/1 M sorbitol	2.8	1.6	3.6	5.3
YEPD/1 M sorbitol → YEPD	3.6	20.3	36.4	19.4

[a] The four strains used were DEY213, DEY217, DEY1032-2C and DEY293-42C.
[b] Cultures were grown in YEPD/1 M sorbitol for 2 hr at 37° and then transferred for a further 2 hr to YEPD with or without sorbitol before staining.

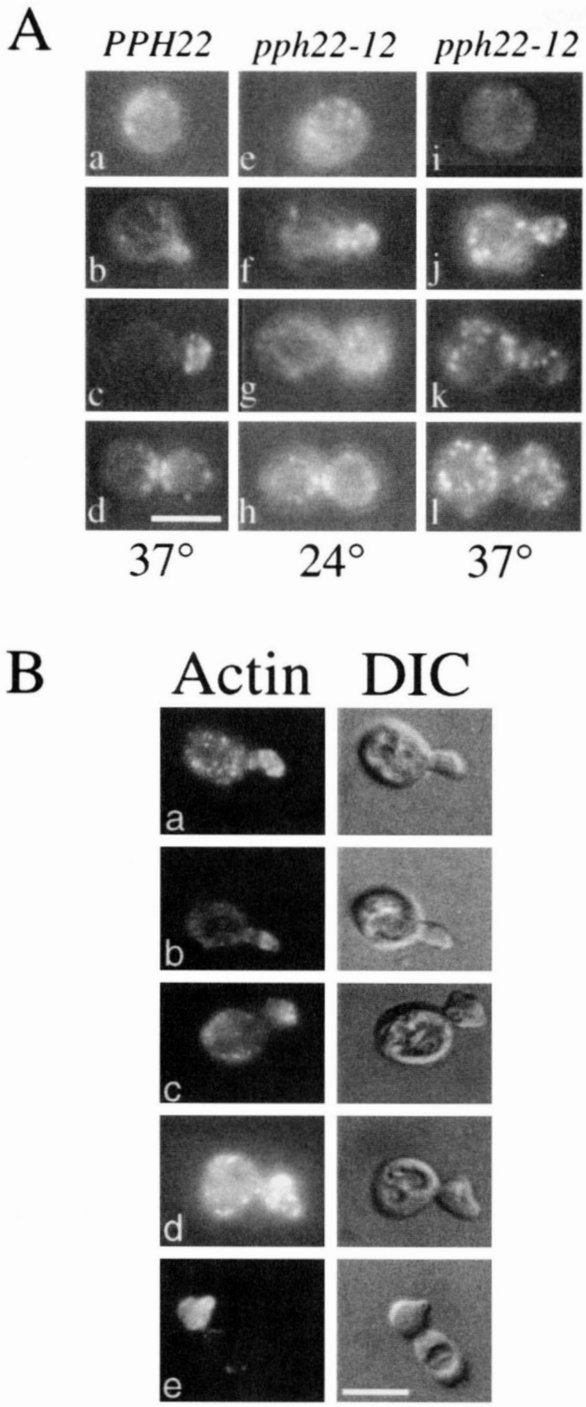

FIGURE 3.—Cortical actin distribution in Ts⁻ *pph22-12* mutant cells. Cells were grown as described in Figure 1 and stained for actin after 4 hr incubation at either 24° or 37° as indicated. (A) At 37°, the cortical actin patches in many *pph22-12* cells are randomly distributed throughout the mother cell and bud. In *PPH22* cells (DEY213) incubated at 37° (a–d) and in *pph22-12* cells (DEY214) incubated at 24° (e–h), cortical actin patches localize to the bud during bud growth or to the mother-bud neck during cytokinesis. In many *pph22-12* mutant cells cortical actin patches are randomly distributed (i–l) at 37°. Bar, 10 μm. (B) At 37°, the cortical actin deposition in many *pph22-12* cells (DEY102D) is hyperpolarized to the region of aberrant bud growth. Cells were stained for actin after 4 hr incubation at 37°. Actin and cell morphology were visualized, respectively, by UV fluorescence and differential interference contrast (DIC) microscopy. Bar, 15 μm.

12 mutant cells was distributed over both the mother cell and the bud (Figure 3A, j–l). Additionally, *pph22-12* mutant cells displaying an aberrant bud morphology at 37° often showed an unusually large deposit of cortical actin at the site of aberrant bud growth (Figure 3B, a–e). *pph22-172* mutant cells displayed similar defects in bud morphogenesis and actin deposition at 37° (not shown). Thus, PP2A loss-of-function caused by mutation of either *PPH21* (LIN and ARNDT 1995) or *PPH22* (this study) interferes with bud morphogenesis and disrupts the cortical actin cytoskeleton.

Ts⁻ *pph22* mutants accumulate binucleate cells: To monitor cell cycle progression in Ts⁻ *pph22* strains, we analyzed their DNA content on shifting from 24° to 37° using flow cytometry. After 3 hr at 37°, *pph22-12* cells showed a predominantly 2N DNA content (Figure 4B). Given that the majority of cells at this time were budded, this is indicative of a cell cycle arrest subsequent to DNA replication but before completion of division. Wild-type populations contained high peaks of both 1N and 2N DNA content at 37° (Figure 4A) as expected for asynchronously cycling cells. In contrast, *pph22-172* cells failed to accumulate with a predominantly 2N DNA content at 37°; instead, the two peaks gradually merged into a single, broad peak with increasing time (Figure 4C). Nevertheless, *pph22-172* cells accumulated with a predominantly 2N DNA content when they were incubated at the lower temperature of 36° (Figure 4D). These results are consistent with the more severe defect of *pph22-172* haploid cells noted above. The significance of the broad peak of fluorescence seen in the more severe mutant after 4–5 hr at 37° is unclear, but could represent a more random arrest of proliferation or result from a more severe osmotic defect at the higher restrictive temperature. Nevertheless, the above results indicate that under appropriate restrictive conditions, both *pph22-12* and *pph22-172* cells block in the cell cycle after S-phase. *pph21-102* cells also block the cell cycle in G2 (LIN and ARNDT 1995), and activation of the mitotic form of the Cdc28p kinase was defective at the restrictive temperature in *pph21-102* cells. Yeast cell cycle progression through mitosis is therefore inhibited by PP2A loss-of-function.

Microscopic analysis of Ts⁻ *pph22* cells incubated at 37° for up to 8 hr revealed a gradual increase in the proportion of cells containing two nuclei within the mother cell (Table 5 and data not shown). Thus the accumulation of cells with a 2N DNA content in Ts⁻ *pph22*-cultures reflects an initial delay in the onset of mitosis, followed by the gradual execution of aberrant nuclear division in which both nuclei are retained in the mother cell. A much higher proportion of binucleate cells at the restrictive temperature was found in the diploid Ts⁻ *pph22-12* strain than in the isogenic haploid (Table 5). Surprisingly, we did not observe a parallel accumulation of anucleate cells in Ts⁻ *pph22* populations at 37°. Since at 4 hr most binucleate cells were budded (data not shown), this suggests that cytokinesis

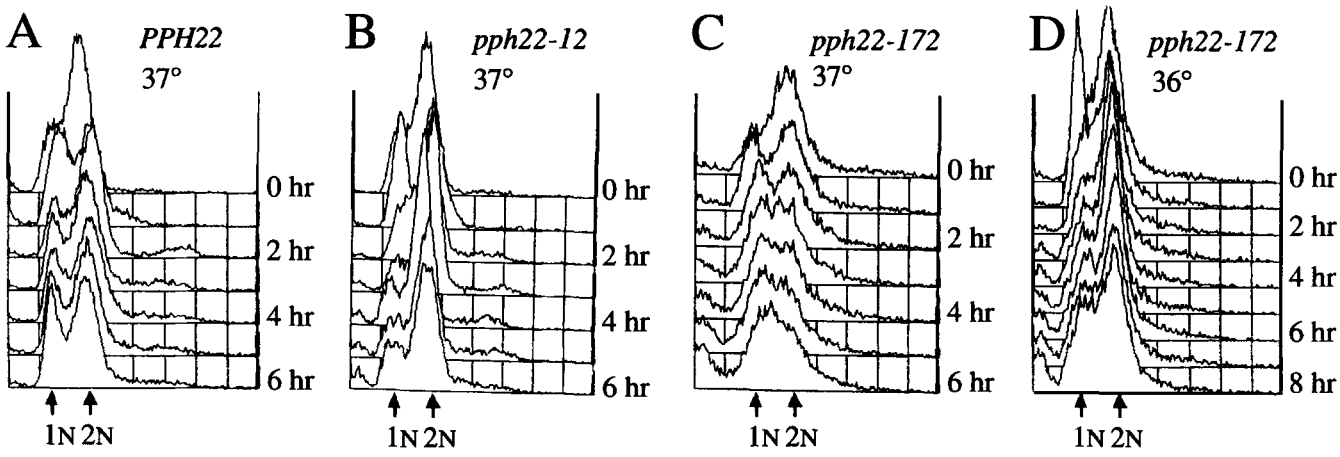

FIGURE 4.—DNA content of Ts⁻ *pph22* mutant cells at different restrictive temperatures. Cells growing actively in liquid YEPD medium at 24° were transferred to either 36° or 37° and sampled hourly for the analysis of DNA content by flow cytometry (MATERIALS AND METHODS). (A) DEY213; (B) DEY214; (C, D) DEY217.

was inhibited following division. By 8 hr (Table 5) around half the binucleate cells were unbudded and frequently very large (Figure 5), suggesting either that aberrant division was also occurring in unbudded cells as happens in *bem2* mutants (KIM *et al.* 1994) or, alternatively, that cytokinesis had taken place but the resulting aploid cell had lysed.

Microtubule organization in Ts⁻ *pph22-12* cells: Indirect immunofluorescence microscopy revealed that in contrast to the wild type, a high proportion of *pph22-12*

TABLE 5

***pph22* mutant cultures accumulate binucleate cells at the restrictive temperature**

			Nuclear morphology (% cells)										
Strain	Genotype	T (°)[a]											
DEY213[b]	*PPH22 (pph3Δ)*	37°	65.2	4.2	<1	13.9	5.1	—	2.1	8.5	—	—	—
DEY214	*pph22-12 (pph3Δ)*	24°	29.2	19.9	—	15.2	10.0	—	8.7	17.0	—	—	—
		37°	34.9	7.1	3.5	9.0	<1	<1	1.9	30.1	2.6	4.8	4.5
DEY102D	*pph22-12/- (pph3Δ/-)*	24°	42.9	13.2	—	24.3	1.8	—	6.0	10.5	<1	<1	—
		37°	37.4	7.5	<1	7.5	<1	<1	<1	15.6	<1	15.6	13.7
DEY217	*pph22-172 (pph3Δ)*	24°	33.8	7.6	—	20.2	6.9	—	8.8	22.1	—	<1	<1
		37°	48.1	4.3	2.8	10.9	1.5	<1	1.2	18.9	<1	4.0	7.1
DEY132-2B[b]	*PPH22 (PPH3)*	37°	59.6	6.1	—	18.7	7.7	—	<1	6.5	—	<1	—
DEY142-1C[c]	*pph22-12 (PPH3)*	37°	37.3	9.0	—	17.1	2.5	—	<1	22.0	—	2.8	8.6
DEY214[c]	*pph22-12 (pph3Δ)*	37°	35.2	6.1	—	12.5	3.4	—	1.5	29.7	—	7.6	3.7
AY925[b,f]	*PPH21 PPH22*	37°	58.1	4.0	—	12.7	2.0	—	<1	21.7	—	<1	<1
DEY1032-2C[d,f]	*pph21Δ pph22Δ*	37°	58.4	3.6	—	3.6	1.2	<1	<1	12.3	—	10.8	9.3
DEY1032-2C[e]	*pph21Δ pph22Δ*	37°	49.8	4.8	—	8.5	2.3	<1	<1	17.4	—	10.0	5.1

The three sections of the table present the results of three separate experiments. In each case, cell cultures growing actively in YEPD medium at 24° were split and incubated for 8 hr at either 24° or 37°. Cells were then fixed and stained with DAPI and the nuclear DNA was visualized by fluorescence microscopy.

[a] Incubation temperature of culture.

[b] Data for nuclear structure were similar at 24° and 37° and therefore, only those obtained at 37° are shown.

[c–e] Culture accumulated approximately 1% (*c*), 2.6% (*d*), 6.1% (*e*) binucleate cells at 24°.

[f] Cells were grown in YEPD medium containing 1 M sorbitol.

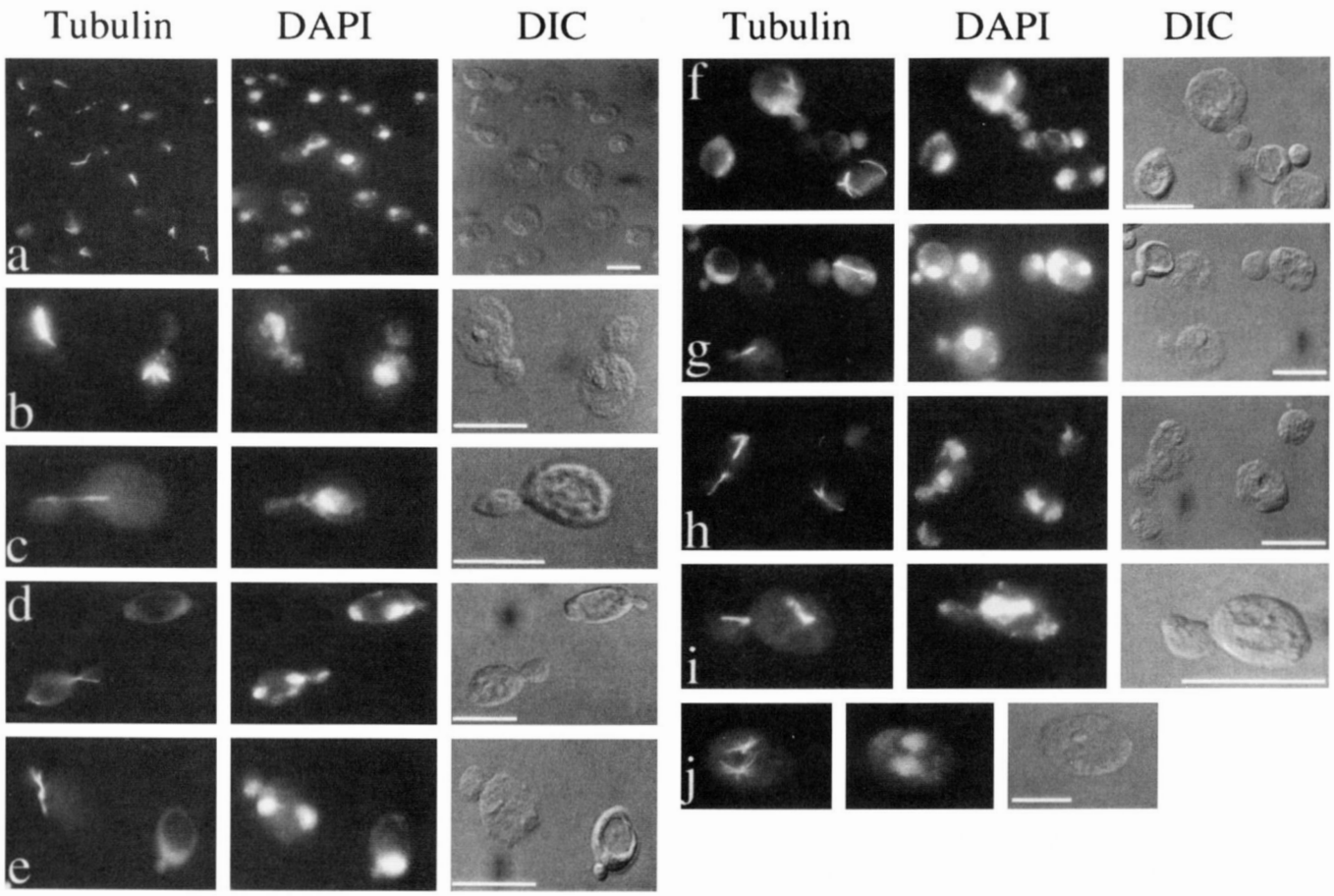

FIGURE 5.—*pph22-12* mutant cells contain multiple nuclei and aberrant microtubule structures at 37°. Cells growing actively in liquid YEPD medium at 24° were transferred to 37° and incubated for a further 4 hr. Cells were then fixed, stained for DNA and tubulin (MATERIALS AND METHODS) and visualized by fluorescence (tubulin and DAPI) or DIC microscopy. (a) wild-type cells (AYS927); (b–j) *pph22-12* mutant cells (DEY102D). Bars, 15 μm.

cells contained multiple and/or aberrant microtubule structures at 37° (Table 6 and Figure 5). Although the efficiency of tubulin staining was lower (~50%) for mutant cells than for wild type, multiple and/or aberrant microtubule structures were observed in both mononucleate (Figure 5, b and i) and binucleate (Figure

TABLE 6

Microtubule organization in *pph22-12* cells at 37°

		Microtubule structure and nuclear morphology (percent cells)															
		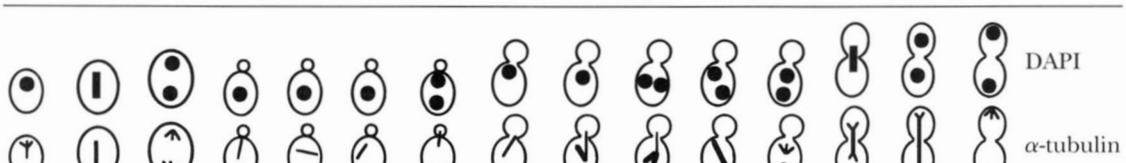															DAPI
		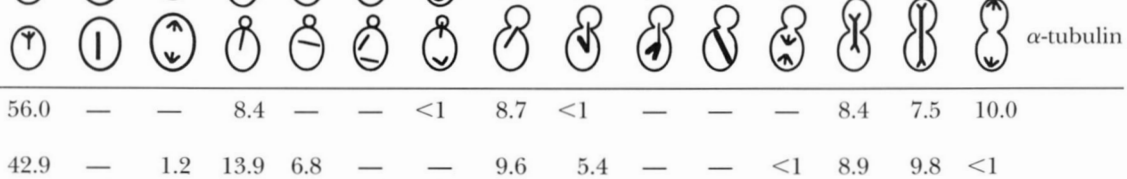															α-tubulin
Strain	T (°)[a]																
PPH22 AYS927	37°	56.0	—	—	8.4	—	—	<1	8.7	<1	—	—	—	8.4	7.5	10.0	
pph22-12 DEY102D	24°	42.9	—	1.2	13.9	6.8	—	—	9.6	5.4	—	—	<1	8.9	9.8	<1	
	37°	33.7	1.0	14.1	7.7	2.5	1.5	2.5	4.3	4.6	2.1	1.1	<1	3.1	19.3	<1	

Cells growing actively in YEPD medium at 24° were split into two cultures and incubated for 8 hr at either 24° or 37°. Cells were then fixed and stained for DNA (DAPI) and tubulin (α-tubulin). At least 300 cells per culture sample were analyzed by fluorescence microscopy to determine the percentage of cells containing both multiple nuclei and aberrant microtubule arrangements.

[a] Incubation-temperature of culture. For strain AYS927, the data obtained for cultures incubated at 24° and 37° were similar and therefore only the data for the culture incubated at 37° are shown.

5, d, f, h and j) *pph22-12* cells at 37°, but not at 24° (Table 6). In some mutant cells, spindle migration occurred in the absence of nuclear migration (Figure 5c). Furthermore, some binucleate mutant cells contained a spindle structure associated with only one nuclear mass (Figure 5e) and some contained an elongated spindle confined to the mother cell (Figure 5g). Some unbudded cells in the *pph22-12* mutant population were very large and contained two nuclei with associated cytoplasmic microtubule structures (Figure 5j), suggesting a defect in bud emergence. At semi-permissive growth temperatures, both *pph22-12* and *pph22-172* cells failed to grow on medium containing the microtubule-destabilizing drug benomyl at concentrations of 20 and 15 μg/ml, respectively, whereas wild-type cells grew well at 20 μg/ml benomyl but poorly at 25 μg/ml (not shown). Taken together, the appearance of aberrant microtubule structures in Ts⁻ *pph22* cultures at 37° and their increased sensitivity to benomyl suggests that PP2A loss of function leads to impaired microtubule function.

Comparison of the phenotypes of *pph21Δ pph22Δ* and Ts⁻ *pph22* cells: The *pph22-12* and *pph22-172* alleles are recessive and conditionally lethal, suggesting that they cause PP2A loss-of-function at 37°. If this is true, we might expect *pph21Δ pph22Δ* cells (which lack PP2A function constitutively) to display a similar range of phenotypes to the Ts⁻ mutants. A *pph21Δ pph22Δ* double deletion in the W303 background causes slow growth at 24° and Ts⁻ growth at 35° (Ronne *et al.* 1991; Lin and Arndt 1995; data not shown). When transferred from 24° to 37° in liquid medium, *pph21Δ pph22Δ* cells displayed a partial arrest of proliferation that was not suppressed by 1 M sorbitol (Figure 6A). The arrest of proliferation by *pph21Δ pph22Δ* mutant cells at 37° may be incomplete because they contain a wild-type *PPH3* gene (see below). In medium lacking 1 M sorbitol (Figure 6B), *pph21Δ pph22Δ* mutant cells underwent a rapid loss of viability at 37° (11% viable cells remaining after 8 hr at 37°), whereas in medium containing 1 M sorbitol (Figure 6B), cell viability decreased at a lower rate (50% viable cells remaining after 8 hr at 37°). In contrast, wild-type cells retained viability under all the conditions tested (Figure 6B). *pph21Δ pph22Δ* cultures showed a 12-fold increase in the fraction of cells permeable to trypan blue compared to a wild-type culture (Table 4), indicating a severe defect in cell wall integrity. Like Ts⁻ *pph22* cells, *pph21Δ pph22Δ* cells therefore show an osmotic defect at 37° that contributes strongly to their viability loss at 37°. Reminiscent of the Ts⁻ *pph22* strains, ~19% of *pph21Δ pph22Δ* cells displayed aberrant bud morphology at 37° in YEPD medium (not shown), but unlike Ts⁻ *pph22* strains, ~13% of *pph21Δ pph22Δ* cells also displayed aberrant bud morphology at 24° (not shown). Whereas the bud morphology defect of Ts⁻ *pph22* cells is conditional, that of *pph21Δ pph22Δ* cells is therefore constitutive. Finally, after 8 hr at 37°, 16% of cells in a *pph21Δ pph22Δ* mutant culture accumulated more than one

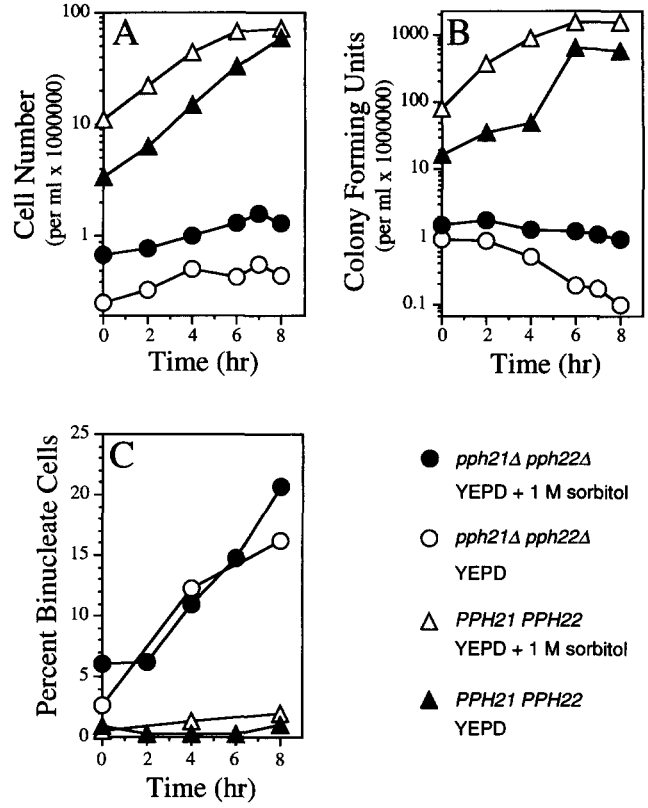

FIGURE 6.—Phenotype of *pph21Δ pph22Δ* mutant cells. Starter cultures were grown to a density of 5–7 × 10^7 cells/ml in YEPD medium containing 1 M sorbitol at 24° then subcultured into YEPD medium containing or lacking 1 M sorbitol and grown for several generations overnight at 24°. Cells growing actively at 24° were transferred to 37° and monitored for cell number (A), colony forming units (B) and the number of nuclei present within the mother cell (C). Serial dilutions for the determination of cell viability were performed in 1 M sorbitol. DNA was stained with DAPI and visualized by fluorescence microscopy. The percentage of binucleate cells in each sample was calculated from the analysis of at least 300 cells. *pph21Δ pph22Δ* (DEY1032-2C); *PPH21 PPH22* (AYS927).

nucleus within the mother cell (Figure 6C and Table 5). Thus, *pph21Δ pph22Δ* cells undergo a defect in nuclear division similar to that observed in Ts⁻ *pph22* strains. Accumulation of binucleate cells in the *pph21Δ pph22Δ* culture occurred regardless of the presence of 1 M sorbitol (Figure 6C and Table 5). Thus, although 1 M sorbitol partially suppresses loss of viability by *pph21Δ pph22Δ* cells at 37°, it fails to suppress their accumulation of multiple nuclei. This supports the conclusion that the osmotic defect of *pph22* cells is the primary cause of their rapid viability loss at 37° and is also consistent with the conclusion that PP2A performs other cellular roles (for example in nuclear division) in addition to its role in the maintenance of cell integrity. Because *pph21Δ pph22Δ* mutant cells display defects in proliferation, osmotic integrity, bud morphogenesis and nuclear division at 37° similar to those observed in Ts⁻ *pph22* strains, we conclude that the phenotype of *pph22-12* and *pph22-172* cells is caused by Pph22p loss-of-function. Furthermore, because the osmotic and nuclear

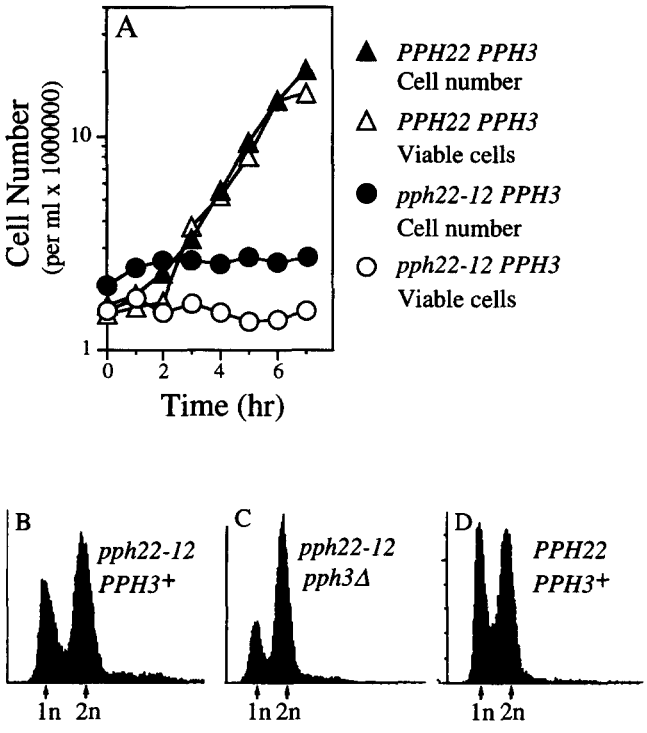

FIGURE 7.—Effect of the *PPH3* gene on the *pph22-12* mutant phenotype. Cells growing actively in liquid YEPD medium at 24° were transferred to 37°. (A) *pph22-12 PPH3* mutant cells arrest proliferation without losing viability at 37°. Cells were monitored hourly for cell density and viability at 37°. (B–D) *pph22-12 PPH3* mutant cells contain both a high 1N and high 2N DNA content after 4 hr at 37°. DNA content was analyzed by flow cytometry. *pph22-12 PPH3* (DEY142-1C); *PPH22 PPH3* (DEY132-2B); *pph22-12 pph3Δ* (DEY214).

division defects of *pph21Δ pph22Δ* cells are more severe at 37° than at 24°, we conclude that PP2A function is especially required for cell integrity and the segregation of replicated DNA during growth at elevated temperatures.

Influence of *PPH3* on the Ts⁻ *pph22* mutant phenotype: *PPH3* gene function is required for cell viability in the absence of *PPH21* and *PPH22* (RONNE *et al.* 1991). This suggests that although the Pph3 phosphatase is not closely related to the *PPH21* and *PPH22* gene products, it performs some overlapping cellular function(s) with PP2A. We therefore investigated the influence of *PPH3* on PP2A rapid loss-of-function by comparing *pph22-12* mutant cells that were either wild type or deleted for *PPH3*. When transferred from 24° to 37° in liquid medium, Ts⁻ *pph22-12 PPH3* mutant cells displayed a range of phenotypes that were similar to those exhibited by Ts⁻ *pph22-12 pph3Δ* mutant cells, including a rapid decrease in the rate of proliferation (Figure 7A), accumulation of binucleate cells (Table 5), suppression by 1 M sorbitol in the growth medium and defects in bud morphogenesis and cortical actin distribution (not shown). Nevertheless, the phenotype of Ts⁻ *pph22-12 PPH3* and *pph22-12 pph3Δ* cells differed in two respects. First, unlike Ts⁻ *pph22-12 pph3Δ* cells that display a tight arrest of proliferation and a rapid loss of viability at 37°, Ts⁻ *pph22-12 PPH3* cells displayed a weak arrest of proliferation at 37° (the cell number doubled approximately three times over 20 hr; not shown) and retained a high level of viability for at least 7 hr at 37° (Figure 7A). Thus, *PPH3* function prevented the rapid viability loss of *pph22-12* mutant cells at 37°, probably through alleviation of their osmotic defect. Secondly, similar to wild-type cultures (Figure 7D) and consistent with a weak arrest of proliferation, *pph22-12 PPH3* cultures displayed high 1N and high 2N DNA peaks at 37° (Figure 7B), indicative of ongoing cell cycle progression. This contrasted with Ts⁻ *pph22-12 pph3Δ* cells, which accumulated predominantly with 2N DNA at 37° (Figure 7C). *PPH3* function therefore suppresses the mitotic delay caused by the *pph22-12* mutation at 37°, but not the eventual accumulation of binucleate cells. Moreover, because *pph21Δ pph22-12* cells display a bud morphogenesis defect regardless of *PPH3* function, this result suggests that the mitotic delay in *pph21Δ pph22-12 pph3Δ* cells at 37° (Figure 7C) is not a response to defective bud growth. Finally, although *PPH3* modifies the Ts⁻ *pph22* phenotype, high copy *PPH3* (on vector YEp351) failed to suppress the growth defect of Ts⁻ *pph22-12* mutant cells incubated on solid medium at 37° (not shown), consistent with the notion that Pph3p function is qualitatively different from that of PP2A.

Effect of *SSD1-v1* on the Ts⁻ *pph22* phenotype: Sit4p displays 55% amino acid sequence identity with the mammalian PP2A C subunit. Defects caused by *sit4* mutations are partially suppressed both by *SSD1-v* (but not *ssd1-d*) alleles of the polymorphic *SSD1* gene and by *PPH22* at high dosage (SUTTON *et al.* 1991). Since both *SSD1-v1* and *PPH22* display genetic interaction with *SIT4* and because our *pph22* mutations were constructed in an *ssd1-d2* background, we examined the influence of the *SSD1-v1* allele on the Ts⁺ *pph22* phenotype. First, we introduced a low copy *SSD1-v1* plasmid into a *pph22-12* mutant strain (DEY102D) and examined cell growth at 37°. Remarkably, at 37° the growth rate of *pph22-12* mutant cells containing the *SSD1-v1* plasmid was similar to that of those containing a *PPH22* plasmid as a control (Figure 8A). In contrast, *pph22-12* mutant cells containing the empty vector (Figure 8A) or cured of the *SSD1-v1* plasmid (not shown) arrested proliferation at 37°. Moreover, like wild-type *PPH22*, low copy *SSD1-v1* suppressed both the aberrant bud morphology and abnormal actin distribution of *pph22-12* cells (not shown). Next, we examined the effect of *SSD1-v1* on cell growth at a range of temperatures in the absence of both *PPH21* and *PPH22* by introducing the *SSD1-v1* plasmid into a *pph21Δ pph22Δ PPH3* double deletion strain (DEY1032-2C). Remarkably, *pph21Δ pph22Δ* mutant cells containing the *SSD1-v1* plasmid grew well at 35° (Figure 8B, a) and slowly at 37° (not shown), whereas *pph21Δ pph22Δ* mutant cells containing the empty vector failed to grow at either temperature. As expected, mutant cells containing a *PPH22*

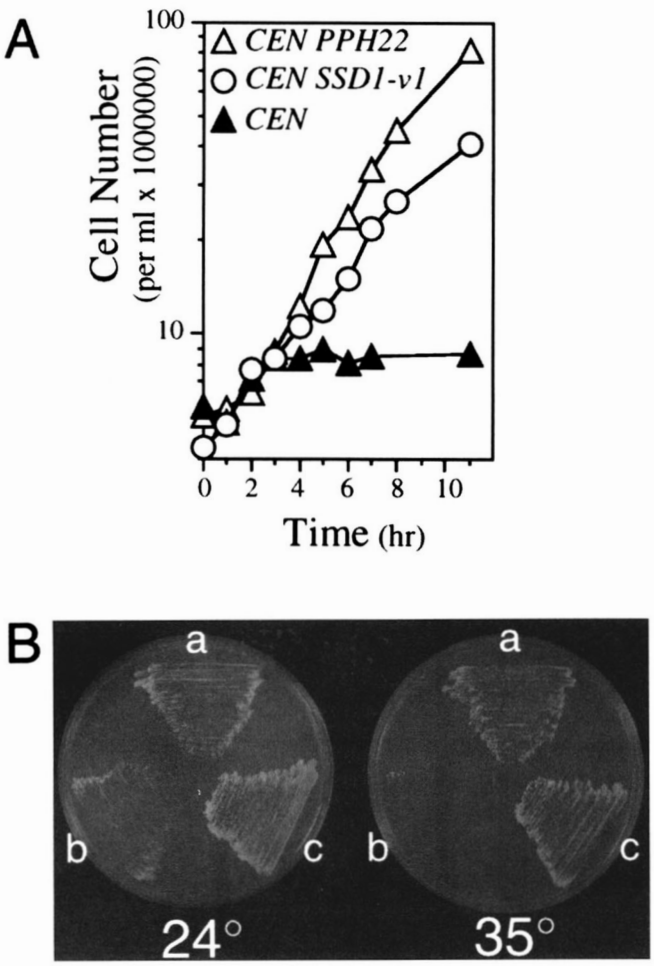

FIGURE 8.—Effect of *SSD1-v1* on Ts$^-$ *pph22* strains. (A) Growth of *pph22-12* mutant cells containing the *SSD1-v1* allele at 37°. *pph22-12* (DEY102D) transformants containing different *CEN* plasmids were grown to a cell density of 1–3 × 10^6/ml in selective medium lacking tryptophan at 24°, transferred to 37° and monitored hourly for cell density. *CEN PPH22* (YCpDE22); *CEN SSD1-v1* (YCpDE24); *CEN* (pRS314). (B) *SSD1-v1* suppresses the temperature sensitivity of *pph21*Δ *pph22*Δ mutant cells at 35°. *pph21*Δ *pph22*Δ (DEY1032-2C) transformants, containing different *CEN* plasmids were struck out on YEPD medium and incubated for 3 days at either 24° or 35°. (a) plasmid pTS64 [*SSD1-v1 LEU2*]; (b) pRS315 [*LEU2*]; (c) YCpDE22 [*PPH22 LEU2*].

plasmid displayed wild-type growth at 37° (Figure 8B, b and c). We also examined the formation of binucleate cells in the double deletion strain carrying *SSD1-v1* after shift to 37°. Regardless of the presence of *SSD1-v1,* the double deletion strain showed a relatively high level of binucleate cells (~5%) even at 24°. However, there was no increase in this level at 37° over 7 hr in the presence of *SSD1-v1.* By comparison, without *SSD1-v1* the fraction of binucleate cells rose to around 25% over 7 hr (data not shown). Thus, *SSD1-v1* partially suppresses all of the major defects caused by absence of the PP2A C subunit.

Finally, we investigated the influence of *SSD1-v1* on growth in the absence of both the PP2A C subunits and Pph3p, using plasmid shuffling to test whether a *TRP1* *SSD1-v1* plasmid could substitute for a *URA3 PPH22* plasmid in the triple *pph* deletion strain DEY3. Transformants containing the *SSD1-v1* plasmid yielded no Ura$^+$ segregants when plated on medium containing 5-FOA, whereas transformants containing a *TRP1 PPH22* plasmid generated Ura$^+$ segregants at high frequency (not shown). Consistently, we have been unable to generate viable *pph21*Δ *pph22*Δ *pph3*Δ [*CEN SSD1-v1*] segregants via tetrad dissection (data not shown). Thus *SSD1-v1* suppresses complete PP2A loss-of-function only in the presence of wild-type *PPH3.*

DISCUSSION

Novel mutant alleles of *PPH22*: We have generated nine novel, temperature-sensitive alleles of the yeast PP2A C subunit gene *PPH22* and have characterized the phenotypic effects of two, *pph22-12* and *pph22-172,* each of which encode single amino acid substitutions within Pph22p. The *pph22-12* and *pph22-172* alleles are recessive, and cells containing either mutation display a rapid arrest of proliferation upon transfer from 24° to 37°. Thus, the *pph22-12* and *pph22-172* mutations are likely to cause a rapid loss of PP2A function. Consistently, a *pph21*Δ *pph22*Δ double deletion strain showed defects at 37° similar to those caused by the *pph22-12* and *pph22-172* mutations. Nevertheless, the Ts$^-$ *pph22* strains are true conditional mutants, displaying wild-type characteristics at 24° and a mutant phenotype at 37°, whereas *pph21*Δ *pph22*Δ deletion-mutant cells are constitutively defective for growth. The constitutive phenotype of *pph21*Δ *pph22*Δ cells makes them prone to accumulate suppressor mutations (RONNE *et al.* 1991), limiting their usefulness for genetic analysis. By comparison, Ts$^-$ *pph22* strains should display genetic stability because their routine growth can be performed under permissive conditions where suppressor mutations are unlikely to confer a growth advantage. As evidence of this, when a haploid *pph22-12* strain was transformed to temperature resistance using a YEp-based gene library, growth at 37° was plasmid-dependent in all Ts$^+$ isolates. The Ts$^-$ *pph22* strains should therefore be valuable tools for functional analysis of PP2A in *S. cerevisiae.*

Mutational changes to the Pph22 polypeptide: The *pph22-12* and *pph22-172* alleles encode single amino-acid substitutions, F232S and P240H, respectively. Both Phe232 and Pro240 are very highly conserved residues that flank a histidine-glycine-glycine tripeptide (residues 235–237 in Pph22p) that is invariant among the catalytic subunits encoded by the PPP gene family (BARTON *et al.* 1994; COHEN 1994), although Sit4p, ppe1 and PPV have leucine at the corresponding position to Phe232. His235 in Pph22p corresponds to His173 in human PP1 and based upon the crystal structure of the latter has been proposed to ligand a Mn^{2+} ion that is critical for catalytic activity (EGLOFF *et al.* 1995). Thus the amino acid changes encoded by the *pph22-12* and

pph22-172 most likely alter an important functional region within the PP2A C subunit. A third mutant allele (*pph22-19*) encodes two amino acid substitutions, N297Y and D347E. While Asn297 and Glu347 are conserved in all PP2A and most PP2A-related protein phosphatases, neither are highly conserved throughout the PPP family, although Asn297 is adjacent to an invariant Phe residue (BARTON *et al.* 1994). In the human PP1 structure, the corresponding residues are close neither to the active site nor to each other (EGLOFF *et al.* 1995). Since neither amino acid substitution alone causes temperature sensitivity, perhaps the combination of both substitutions causes Ts$^-$ growth by promoting general structural destabilization of the protein at the restrictive temperature. A similar phenomenon has been observed in *prt1*^{ts} alleles (EVANS *et al.* 1995).

PP2A and cell wall integrity: Since Ts$^-$ *pph22* cells show an aberrant distribution of the actin cytoskeleton and defective bud morphogenesis at 37°, it is possible that PP2A performs an indirect role in the maintenance of cell integrity via regulation of cytoskeletal components. *TCP1* encodes a protein thought to link regulation of both microfilaments and microtubules and, like Ts$^-$ *pph22* cells, *tcp1* mutants display aberrant actin structures, abnormal microtubules and an accompanying cell wall defect (URSIC *et al.* 1994). However, a more direct role for PP2A in controlling cell integrity is suggested by genetic interactions between PP2A and *BEM2*, a gene involved in bud growth (BENDER and PRINGLE 1989). Thus, *bem2* mutations can suppress *cdc55-1* (HEALY *et al.* 1991), while *BEM2* deletion is synthetically lethal in combination with simultaneous deletion of *PPH21* and *PPH22* (LIN and ARNDT 1995). *BEM2* encodes the GTPase-activating protein for the small G protein encoded by *RHO1* (PETERSON *et al.* 1994; KIM *et al.* 1994). Rho1p regulates cell wall biosynthesis both as a component of $\beta(1\rightarrow3)$glucan synthase (DRGONOVA *et al.* 1996; QADOTA *et al.* 1996) and by activation of Pkc1p (NONAKA *et al.* 1995; KAMADA *et al.* 1996), a protein kinase C homologue that in turn regulates the Mpk1p MAP kinase signal transduction pathway required for cell wall integrity and polarized cell growth (see ERREDE and LEVIN 1993). In fact *bem2* mutants and the Ts$^-$ *pph22* strains appear to share many common phenotypic features. Like Ts$^-$ *pph22* cells, *bem2* mutants display a temperature-dependent disruption of the actin cytoskeleton, a bud growth defect, a sorbitol-remedial Ts$^-$ cell lysis defect and the accumulation of binucleate cells at the restrictive temperature (WANG and BRETSCHER 1995).

We have looked for genetic interaction between our Ts$^-$ mutants and components of the Pkc1p/Mpk1p pathway to examine whether the cell wall integrity defect of Ts$^-$ *pph22* strains might be mediated by this route. Mutations in Pkc1p or components of the downstream MAP kinase pathway (Bck1p, Mkk1p/Mkk2p, Mpk1p) confer a Ts$^-$ cell lysis defect, and elevated gene dosage at each level of the pathway can compensate for upstream defects (ERREDE and LEVIN 1993). However, high copy *MPK1*, *MKK1* or *PKC1* (and the constitutively activated *BCK1-20* allele) each failed to suppress the *pph22* Ts$^-$ growth defect, suggesting that PP2A loss of function does not inactivate this signalling pathway. Nonetheless, while both *mpk1::TRP1* and the Ts$^-$ *pph22-172* strains can grow at 35° in the presence of 1 M sorbitol, the isogenic Ts$^-$ *pph22-172 mpk1::TRP1* strain cannot (data not shown). This synthetic growth defect provides additional support for the notion that Ts$^-$ *pph22* strains are impaired for cell wall integrity. Taken together, these data suggest that PP2A loss of function may block a pathway required in parallel to Pkc1p-Mpk1p for cell integrity but are also consistent with possible roles downstream of Mpk1p.

***SSD1-v1* and the Ts$^-$ *pph22* phenotype:** The strong suppression of Ts$^-$ *pph22* phenotypes by *SSD1-v1* is consistent with the role of PP2A in bud growth. *SSD1-v1* suppresses mutations in a large number of genes involved in morphogenesis and cell surface growth (see DOSEFF and ARNDT 1995), including those in *MPK1* (LEE *et al.* 1993), *BCK1/SLK1* (COSTIGAN *et al.* 1992) and *BEM2/IPL2* (KIM *et al.* 1994), genes implicated in control of cell wall synthesis, as well as mutations in the *SIT4* (SUTTON *et al.* 1991), *SWI4* (NASMYTH and DIRICK 1991) and *CLN1/CLN2* (CVRCKOVA and NASMYTH 1993) genes, which are required for exit from G1 and bud emergence. *SSD1-v1* also suppresses the growth defects caused by hyperactivation of the Ras/protein kinase A pathway controlling nutrient sensing and cell proliferation (WILSON *et al.* 1991). Ssd1p contains a sequence motif that is highly conserved in a number of proteins implicated in RNA processing, some of which possess 3′–5′ exoribonuclease activity (see TURCQ *et al.* 1992; DOSEFF and ARNDT 1995; DMOCHOWSKA *et al.* 1995). *SSD1-v* function may therefore be required for a post-transcriptional control mechanism (DOSEFF and ARNDT 1995), suppressing *pph22* mutations indirectly by reversing an effect of those mutations on gene expression. However, *SSD1-v1* suppression of the effects of PP2A loss-of-function requires at least some residual phosphatase activity because *SSD1-v1* failed to suppress the effects of a *pph21*Δ *pph22*Δ double deletion in the absence of *PPH3*. Thus Ssd1p might act more directly to stimulate the activity of PP2A or PP2A-related phosphatases against substrate(s) whose hyperphosphorylation leads to growth defects in the mutant cells.

***PPH22* and nuclear division:** Our data support the notion that loss of Pph22p function leads to a block before mitosis, such that cells accumulate with replicated DNA but do not progress to timely nuclear division. This is fully consistent with the experiments of LIN and ARNDT (1995), who showed that loss of PP2A function in a Ts$^-$ *pph21-102* strain leads to a G2 arrest because activation of the mitotic Clb·Cdc28 protein kinase is blocked. However, our data show that the block to mitosis is not absolute in Ts$^-$ *pph22* cells; after ~4 hr, some cells enter mitosis and segregate two nu-

clear masses, often becoming binucleate. It is possible that the block to mitosis in Ts⁻ *pph22* cells is due to engagement of a checkpoint control in response to defective microtubule organization, but that this control ultimately fails so that some cells can undergo aberrant division to give binucleate cells. In this case, it is possible that PP2A may be required for the maintenance of such a checkpoint. It will be interesting to determine whether *pph21-102* and Ts⁻ *pph22* mutant cells display a difference in the permanency of their mitotic blocks because of gene- or allele-specific differences or differences in experimental regimes.

In principle, the generation of binucleate cells could result from the defect in bud growth in Ts⁻ *pph22* cells at 37°, since DNA segregation between the mother and daughter cell might be difficult in the absence of a properly formed bud. However, *pph22-12* cells display abnormal microtubule structures at 37° (Figure 5), a significant fraction of cells containing multiple spindle structures and/or showing misalignment of the spindle with the mother-bud axis. Moreover, some *pph22-12* cells contained aberrant microtubule structures that were either fragmented or dissociated from the nuclear mass. In mammalian cells PP2A associates with microtubules and the microtubule-associated PP2A activity is cell-cycle regulated (SONTAG *et al.* 1995), suggesting that PP2A may regulate microtubule dynamics in this system. Nevertheless, *S. cerevisiae* tubulin mutants generally do not accumulate binucleate cells, although the cold-sensitive *tub2-401* mutant (mutated in the β-tubulin gene) displays a binucleate phenotype similar to that shown by Ts⁻ *pph22* cells (PALMER *et al.* 1992). The increase in frequency of *tub2-401* binucleate cells at 18° occurs because of a specific loss of cytoplasmic microtubules, which, in turn, causes a failure in the proper orientation of the intact mitotic spindle. However, since many binucleate Ts⁻ *pph22* mutant cells contain prominent astral microtubules at 37° (see, for example, Figure 5j; Table 6), if the defects in microtubule function are responsible for production of binucleate cells, then loss of cytoplasmic microtubules would not appear to be the cause. Since 1 M sorbitol strongly suppressed the viability loss of the *pph21Δ pph22Δ* strain without any noticeable effect on the rate of formation of binucleate cells (see Table 5 and Figure 6), the aberrant nuclear division in PP2A-deficient cells cannot simply be a result of their lysis defect.

In addition to astral microtubule function, proper orientation of the yeast mitotic spindle requires the function of the actin cytoskeleton. Thus, Ts⁻ *act1-4* mutant cells (mutated in the actin structural gene) undergo disruption of the actin cytoskeleton at 37° and as a result, misorient the mitotic spindle and accumulate multiple nuclei despite the presence of astral microtubules (PALMER *et al.* 1992). The defective microtubule function and accumulation of multiple nuclei in Ts⁻ *pph22* mutant cells may therefore be an indirect consequence of disruption of the actin cytoskeleton. This notion is supported by the fact that disruption of the actin cytoskeleton in *bem2* cells at 37° is also accompanied by accumulation of multiple nuclei (WANG and BRETSCHER 1995).

We thank WOLFGANG HILT, DAVID LEVIN, KUNIHIRO MATSUMOTO and HANS RONNE for providing materials used in this study and the CRC Nucleic Acid Structure Group at Dundee for the synthesis of oligonucleotides. We are particularly grateful to ALAN SNEDDON for making the *pph3::LYS2* construct. We also thank PAUL ANDREWS for reading the manuscript. The research benefited from use of the SEQNET facility at Daresbury, U.K. This work was carried out with support from the Wellcome Trust (project grant 039042/1.5 to M.J.R.S.).

LITERATURE CITED

ADAMS, A. E. M., and J. R. PRINGLE, 1984 Relationship of actin and tubulin distribution to bud growth in wild-type and morphogenetic mutant *Saccharomyces cerevisiae*. J. Cell Biol. **98:** 934–945.

BARTON, G. J., P. T. W. COHEN and D. BARFORD, 1994 Conservation analysis and structure prediction of the serine/threonine phosphatases. Eur. J. Biochem. **220:** 225–237.

BENDER, A., and J. R. PRINGLE, 1989 Multicopy suppression of the *cdc24* budding defect in yeast by *CDC42* and three newly identified genes including the *ras*-related gene *RSR1*. Proc. Natl. Acad. Sci. USA **86:** 9976–9980.

BERBEN, G., J DUMONT, V. GILLIQUET, P.-A. BOLLE and F. HILGER, 1991 The YDp plasmids: a uniform set of vectors bearing versatile gene disruption cassettes for *Saccharomyces cerevisiae*. Yeast **7:** 475–477.

BUTLER, A. R., J. H. WHITE and M. J. R. STARK, 1991 Analysis of the response of *Saccharomyces cerevisiae* cells to *Kluyveromyces lactis* toxin. J. Gen. Microbiol. **137:** 1749–1757.

CHANT, J., 1994 Cell polarity in yeast. Trends Genet. **10:** 328–333.

CID, V. J., DURAN, F. DEL REY, M. P. SNYDER, C. NOMBELA *et al.*, 1995 Molecular basis of cell integrity and morphogenesis in *Saccharomyces cerevisiae*. Microbiol. Rev. **59:** 345–386.

COHEN, P., 1989 The structure and regulation of protein phosphatases. Annu. Rev. Biochem. **58:** 453–508.

COHEN, P. T. W., 1994 Nomenclature and chromosomal localization of human protein serine/threonine phosphatase genes. Adv. Prot. Phosphatases **8:** 371–376.

COHEN, P., D. L. SCHELLING and M. J. R. STARK, 1989 Remarkable similarities between yeast and mammalian protein phosphatases. FEBS Letts. **250:** 601–606.

COSTIGAN, C., S. GEHRUNG and M. SNYDER, 1992 A synthetic lethal screen identifies SLK1, a novel protein kinase homolog implicated in yeast cell morphogenesis and cell growth. Mol. Cell. Biol. **12:** 1162–1178.

COSTIGAN, C., D. KOLODRUBETZ and M. SNYDER, 1994 *NPH6A* and *NPH6B*, which encode HMG1-like proteins, are candidates for downstream components of the the *SLT2* mitogen-activated protein kinase pathway. Mol. Cell. Biol. **14:** 2391–2403.

CVRCKOVA F., and K. NASMYTH, 1993 Yeast G_1 cyclins *CLN1* and *CLN2* and a GAP-like protein have a role in bud formation. EMBO J. **12:** 5277–5286.

DMOCHOWSKA, A., P. GOLIK and P. P. STEPIEN, 1995 The novel nuclear gene DSS-1 of *Saccharomyces cerevisiae* is necessary for mitochondrial biogenesis. Curr. Genet. **28:** 108–112.

DOSEFF, A. I., and K. T. ARNDT, 1995 LAS1 is an essential nuclear protein involved in cell morphogenesis and cell surface growth. Genetics **141:** 857–871.

DRGONOVA, J., T. DRGON, K. TANAKA, R. KOLLAR, G.-C. CHEN *et al.*, 1996 Rho1p, a yeast protein at the interface between cell polarization and morphogenesis. Science **272:** 277–279.

EGLOFF, M. P., P. T. W. COHEN, P. REINEMER and D. BARFORD, 1995 Crystal structure of the catalytic subunit of human protein phosphatase 1 and its complex with tungstate. J. Mol. Biol. **254:** 942–959.

ERREDE, B., and D. E. LEVIN, 1993 A conserved kinase cascade for MAP kinase activation in yeast. Curr. Biol. **5:** 254–260.

EVANS, D. R. H., C. RASMUSSEN, P. J. HANIC-JOYCE, G. C. JOHNSTON, R. A. SINGER *et al.*, 1995 Mutational analysis of the Prt1 protein subunit of yeast translation initiation factor 3. Mol. Cell. Biol. **15:** 4525–4535.

FERNANDEZ-SARABIA, M. J., A. SUTTON, T. ZHONG and K. T. ARNDT, 1992 SIT4 protein phosphatase is required for the normal accumulation of *SWI4, CLN1, CLN2* and *HCS26* RNAs during late G1. Genes Dev. **6:** 2417–2428.

GIETZ, R. D., and A. SUGINO, 1988 New yeast-*Escherichia coli* shuttle vectors constructed with *in vitro* mutagenized yeast genes lacking six-base pair restriction sites. Gene **74:** 527–534.

HEALY, A. M., S. ZOLNIEROWICZ, A. E. STAPLETON, M. GOEBL, A. A. DEPAOLI-ROACH *et al.,* 1991 *CDC55,* a *Saccharomyces cerevisiae* gene involved in cellular morphogenesis: identification, characterization and homology to the B subunit of mammalian type 2A protein phosphatase. Mol. Cell. Biol. **11:** 5767–5780.

HOFFMANN, R., S. JUNG, M. EHRMANN and H. W. HOFER, 1994 The *Saccharomyces cerevisiae* gene *PPH3* encodes a protein phosphatase with properties different from *PPX, PP1* and *PP2A.* Yeast **10:** 567–578.

KAISER, C., S. MICHAELIS and A. MITCHELL, 1994 *Methods in Yeast Genetics,* Cold Spring Harbor Laboratory, Cold Spring Harbor, NY.

KAMADA, Y., H. QADOTA, C. P. PYTHON, Y. ANRAKU, Y. OHYA *et al.,* 1996 Activation of yeast protein kinase C by Rho1 GTPase. J. Biol. Chem. **271:** 9193–9196.

KARPOVA, T. S., M. M. LEPETIT and J. A. COOPER, 1993 Mutations that enhance the *cap2* null mutant phenotype in *Saccharomyces cerevisiae* affect the actin cytoskeleton, morphogenesis and pattern of growth. Genetics **135:** 693–709.

KILMARTIN, J., and A. E. M. ADAMS, 1984 Structural rearrangements of tubulin and actin during the cell cycle of the yeast *Saccharomyces cerevisiae.* J. Cell Biol. **98:** 922–933.

KIM, Y.-J., L. FRANCISCO, G.-C. CHEN, E. MARCOTTE and C. S. M. CHAN, 1994 Control of cellular morphogenesis by Ipl2/Bem2 GTPase-activating protein: possible role of protein phosphorylation. J. Cell Biol. **127:** 1381–1394.

KINOSHITA, N., H. OHKURA and M. YANAGIDA, 1990 Distinct, essential roles of type 1 and 2A protein phosphatases in the control of the fission yeast cell division cycle. Cell **63:** 405–415.

KINOSHITA, N., M. GOEBL and M. YANAGIDA, 1991 The fission yeast *dis3*$^+$ gene encodes a 110-kDa essential protein implicated in mitotic control. Mol. Cell. Biol. **11:** 5839–5847.

KINOSHITA, N., H. YAMANO, H. NIWA, T. YOSHIDA and M. YANAGIDA, 1993 Negative regulation of mitosis by the fission yeast protein phosphatase ppa2. Genes Dev. **7:** 1059–1071.

KINOSHITA, K., T. NEMOTO, K. NABESHIMA, H. KONDOH, H. NIWA *et al.,* 1996 The regulatory subunits of fission yeast protein phosphatase 2A (PP2A) affect cell morphogenesis, cell wall synthesis and cytokinesis. Genes Cells **1:** 29–45.

LEE, K. S., K. IRIE, Y. GOTOH, Y. WATANABE, H. ARAKI *et al.,* 1993 A yeast mitogen-activated protein kinase homolog (Mpk1) mediates signalling by protein kinase C. Mol. Cell. Biol. **13:** 3067–3075.

LEE, T. H., M. J. SOLOMON, M. C. MUMBY and M. W. KIRSCHNER, 1991 INH, a negative regulator of MPF, is a form of protein phosphatase 2A. Cell **64:** 415–423.

LEE, T. H., C. TURCK and M. W. KIRSCHNER, 1994 Inhibition of cdc2 activation by INH/PP2A. Mol. Cell. Biol. **5:** 323–338.

LEUNG, D. W., E. CHEN and D. V. GOEDDEL, 1989 A method for random mutagenesis of a defined DNA segment using a modified polymerase chain reaction. Technique A. J. Cell. Mol. Biol. **1:** 11–15.

LEW D. J., and S. I. REED, 1993 Morphogenesis in the yeast cell cycle: regulation by Cdc28 and cyclins. J. Cell Biol. **120:** 1305–1320.

LIN, F. C., and K. ARNDT, 1995 The role of *Saccharomyces cerevisiae* type 2A phosphatase in the actin cytoskeleton and in entry into mitosis. EMBO J. **14:** 2745–2759.

MAYER-JAEKEL, R. E., H. OHKURA, R. GOMES, C. E. SUNKEL, S. BAUMGARTNER *et al.,* 1993 The 55 kd regulatory subunit of Drosophila protein phosphatase 2A is required for anaphase. Cell **72:** 621–633.

MUHLRAD, D., R. HUNTER and R. PARKER, 1992 A rapid method for localized mutagenesis of yeast genes. Yeast **8:** 79–82.

NASMYTH, K., and L. DIRICK, 1991 The role of SWI4 and SWI6 in the activity of G1 cyclins in yeast. Cell **66:** 995–1013.

NONAKA, H., K. TANAKA, H. HIRANO, T. FUJIWARA, H. KOHNO *et al.,* 1995 A downstream target of *RHO1* small GTP-binding protein is *PKC1,* a homolog of protein kinase C, which leads to activation of the MAP kinase cascade in *Saccharomyces cerevisiae.* EMBO J. **14:** 5931–5938.

PALMER, R. E., D. S. SULLIVAN, T. HUFFAKER and D. KOSHLAND, 1992 Role of astral microtubules and actin in spindle orientation and migration in the budding yeast *Saccharomyces cerevisiae.* J. Cell Biol. **119:** 583–593.

PETERSON, J., Y. ZHENG, L. BENDER, A. MYERS, R. CERIONE *et al.,* 1994 Interactions between the bud emergence proteins Bem1p and Bem2p and Rho-type GTPases in yeast. J. Cell Biol. **127:** 1395–1406.

QADOTA, H., C. P. PYTHON, S. B. INOUE, M. ARISAWA, Y. ANRAKU *et al.,* 1996 Identification of yeast Rho1p GTPase as a regulatory subunit of 1,3-β-glucan synthase. Science **272:** 279–281.

RONNE, H., M. CARLBERG, G.-Z. HU and J. O. NEHLIN, 1991 Protein phosphatase 2A in *Saccharomyces cerevisiae:* effects on cell growth and bud morphogenesis. Mol. Cell. Biol. **11:** 4876–4884.

SAMBROOK, J., E. F. FRITSCH and T. MANIATIS, 1989 *Molecular Cloning: A Laboratory Manual,* Ed. 2. Cold Spring Harbor Laboratory, Cold Spring Harbor, NY.

SCHIESTL, R. H., and R. D. GIETZ, 1989 High efficiency transformation of intact yeast cells using single stranded nucleic acids as a carrier. Curr. Genet. **16:** 339–346.

SIKORSKI, R. S., and P. HIETER, 1989 A system of shuttle vectors and yeast host strains designed for efficient manipulation of DNA in *Saccharomyces cerevisiae.* Genetics **122:** 19–27.

SNEDDON, A. A., P. T. W. COHEN and M. J. R. STARK, 1990 *Saccharomyces cerevisiae* protein phosphatase 2A performs an essential cellular function and is encoded by two genes. EMBO J. **9:** 4339–4346.

SONTAG, E., V. NUNBHAKDI-CRAIG, G. S. BLOOM and M. C. MUMBY, 1995 A novel pool of protein phosphatase 2A is associated with microtubules and is regulated during the cell cycle. J. Cell Biol. **128:** 1131–1144.

SUTTON, A., D. IMMANUEL and K. ARNDT, 1991 The SIT4 protein phosphatase functions in late G_1 for progression into S phase. Mol. Cell. Biol. **11:** 2133–2148.

TURCQ, B., K. F. DOBINSON, N. SERIZAWA and A. M. LAMBOWITZ, 1992 A protein required for RNA processing and splicing in *Neurospora* mitochondria is related to gene products involved in cell cycle protein phosphatase functions. Proc. Natl. Acad. Sci. USA **89:** 1676–1680.

URSIC, D., J. C. SEDBROOK, K. L. HIMMEL and M. R. CULBERTSON, 1994 The essential yeast Tcp1 protein affects actin and microtubules. Mol. Biol. Cell **5:** 1065–1080.

VAN ZYL, W., W. HUANG, A. A. SNEDDON, M. STARK, S. CAMIER *et al.,* 1992 Inactivation of the protein phosphatase 2A regulatory subunit A results in morphological and transcriptional defects in *Saccharomyces cerevisiae.* Mol. Cell. Biol. **12:** 4946–4959.

WANG, T., and A. BRETSCHER, 1995 The *rho*-GAP encoded by *BEM2* regulates cytoskeletal structure in budding yeast. Mol. Biol. Cell **6:** 1011–1024.

WASSERMAN, D. A., N. M. SOLOMON, H. C. CHANG, F. D. KARIM, M. THERRIEN *et al.,* 1996 Protein phosphatase 2A positively and negatively regulates Ras1-mediated photoreceptor development in Drosophila. Genes Dev. **10:** 272–278.

WATANABE, Y., K. IRIE and K. MATSUMOTO, 1995 Yeast *RLM1* encodes a serum response factor-like protein that may function downstream of the Mpk1 (Slt2) mitogen-activated protein kinase pathway. Mol. Cell. Biol. **15:** 5740–5749.

WILSON, R. B., A. A. BRENNER, T. B. WHITE, M. J. ENGLER, J. P. GAUGHRAN *et al.,* 1991 The *Saccharomyces cerevisiae SRK1* gene, a suppressor of *bcy1* and *ins1,* may be involved in protein phosphatase function. Mol. Cell. Biol. **11:** 3369–3373.

ZARZOV, P., C. MAZZONI and C. MANN, 1996 The SLT2(MPK1) MAP kinase is activated during periods of polarized cell growth in yeast. EMBO J. **15:** 83–91.

Communicating editor: A. P. MITCHELL